Viscous cavities

Anne Le Goff, David Quéré, Christophe Clanet

Viscous cavities

Anne Le Goff, David Quéré, and Christophe Clanet

Citation: Physics of Fluids (1994-present) **25**, 043101 (2013); doi: 10.1063/1.4797499
View online: http://dx.doi.org/10.1063/1.4797499
View Table of Contents: http://scitation.aip.org/content/aip/journal/pof2/25/4?ver=pdfcov
Published by the AIP Publishing

PHYSICS OF FLUIDS **25**, 043101 (2013)

Viscous cavities

Anne Le Goff,[1,2] David Quéré,[1,3] and Christophe Clanet[1,3]
[1]*PMMH, UMR 7636 du CNRS, ESPCI, 10 rue Vauquelin, 75005 Paris, France*
[2]*MMN, Gulliver, UMR 7083 du CNRS, ESPCI, 10 rue Vauquelin, 75005 Paris, France*
[3]*LadHyX, UMR 7646 du CNRS, Ecole Polytechnique, 91128 Palaiseau, France*

(Received 3 January 2013; accepted 8 March 2013; published online 4 April 2013)

We study experimentally the impact of solid spheres in a viscous liquid at moderate Reynolds numbers ($Re \sim 5$–100). We first determine the drag force by following the slowdown dynamics of projectiles. We then focus on the shape of the free surface: such impacts generate cavities, whose original shape is described and modeled. © *2013 American Institute of Physics*. [http://dx.doi.org/10.1063/1.4797499]

I. INTRODUCTION

Since the pioneering work of Worthington and Cole,[1] impact of solid projectiles in liquids have kept drawing the attention of researchers,[2,3] from purely theoretical fluid mechanics[4] to applied aeronautics.[5] The corresponding experimental studies mainly involve disks[6,7] and spheres[8,9] impacting water, and they all report the formation of elongated cavities (Figures 1(a) and 1(b)) that pinch off before the projectile stops.[10,11] These studies were extended to more complex fluids, and elongated cavities are also observed as solid spheres impact loose sand,[12–15] foam,[16] or viscoelastic micellar solutions.[17,18] It is tempting to simplify the complex rheology of the fluids by considering viscous Newtonian liquids, which we do in this paper. Fast impacts in such liquids are found to be quite different from commonly observed, as seen in Figure 1 where a comparison is made between the impact cavities generated in a non-viscous and in a viscous liquid, of surface tension either low (a and b) or high (c and d). Compared to what they are in liquids 100–1000 times less viscous, cavities are found to be much wider, with an aspect ratio comparable to unity. As these centimeter-size cavities form, the projectiles stop, which stresses the natural efficiency of viscous liquids to absorb kinetic energy. We describe in the paper the main questions raised by these observations: after presenting the experiments, we successively discuss the arrest distance of the projectile, and the isotropic nature of the cavity in these viscous impacts.

II. EXPERIMENTAL OBSERVATIONS

We mainly use polypropylene spheres of density $\rho_s = 920$ kg/m^3 comparable to that of the liquid. However, we also consider stainless steel ($\rho_s = 7700$ kg/m^3), glass ($\rho_s = 2600$ kg/m^3), and polyacetal ($\rho_s = 1410$ kg/m^3) in order to check the effect of the solid density. The radius R_0 of the projectile ranges from 2 mm to 5 mm. A slingshot is used to reach impact velocities from $V_0 = 10$ m/s up to $V_0 = 60$ m/s. The liquid in the bath is a silicon oil Rhodorsil 47V1000 of dynamic viscosity $\eta = 1$ Pa s, density $\rho = 980$ kg/m^3, and surface tension $\gamma = 0.02$ N/m (ensuring the complete wetting of the spheres). A typical shear rate V_0/R_0 at impact is 10^4 s^{-1}, and then quickly decreases, so that the dynamic viscosity is weakly affected (less than 10% decrease). At such shear rates, glycerol [Figure 1(d)] also behaves as a Newtonian fluid.[19]

The liquids are transparent and the motion of the projectiles is recorded using a high-speed camera (Phantom V7, 1000–10 000 frames/s). The motion is filmed from the side, using backlighting to enhance contrast, which gives access to the projectile deceleration and to the cavity formation and collapse. A typical sequence is presented in Figure 2, which shows the dynamics of a viscous cavity, obtained after a polypropylene sphere ($R_0 = 3.5$ mm) impacted the bath at $V_0 = 28$ m/s. The sphere is almost stopped within the first three frames. The corresponding deceleration can be evaluated to

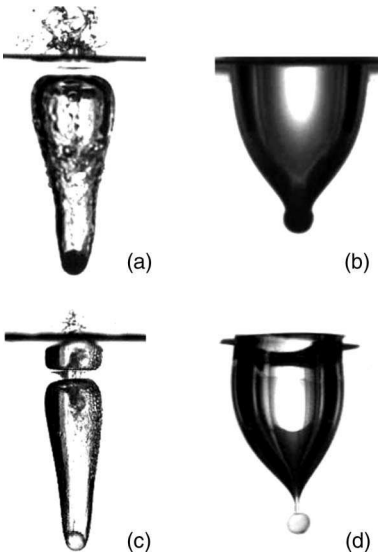

FIG. 1. (a) and (b) Cavities created by a polypropylene sphere of radius $R_0 = 2.4$ mm impacting at $V_0 = 15$ m/s a bath of silicon oil of viscosity (a) $\eta = 10$ mPa s and (b) $\eta = 1000$ mPa s. (c) and (d) Cavities created by a glass sphere of radius $R_0 = 2$ mm after an impact at $V_0 = 18$ m/s onto a bath (c) of water ($\eta = 1$ mPa s) or (d) of pure glycerol ($\eta = 1400$ mPa s).

$28/0.008 \approx 350\ g$. During this short phase of 8 ms, the shape of the cavity is close to a truncated cone. As time increases, the sphere remains at rest while the cavity widens and reaches almost a hemispherical shape at $t = 50$ ms. At that time, it pinches at the north pole of the solid sphere and starts to retract. The retraction lasts 70 ms, leaving the projectile with tiny bubbles in the bath. Since the projectile stops before the cavity retracts, there is no bubble entrainment, contrasting with what is observed at low viscosity.[17,20] Another difference is the absence of cavity pinch-off. In water, a neck roughly appears halfway between the sphere and the free surface, breaking the cavity in two parts.[3,10,20] In viscous liquids, there is no such fragmentation of the entrapped air, that stays in one whole volume (Figure 2). Sections III and IV respectively focus on the deceleration phase and on the cavity dynamics.

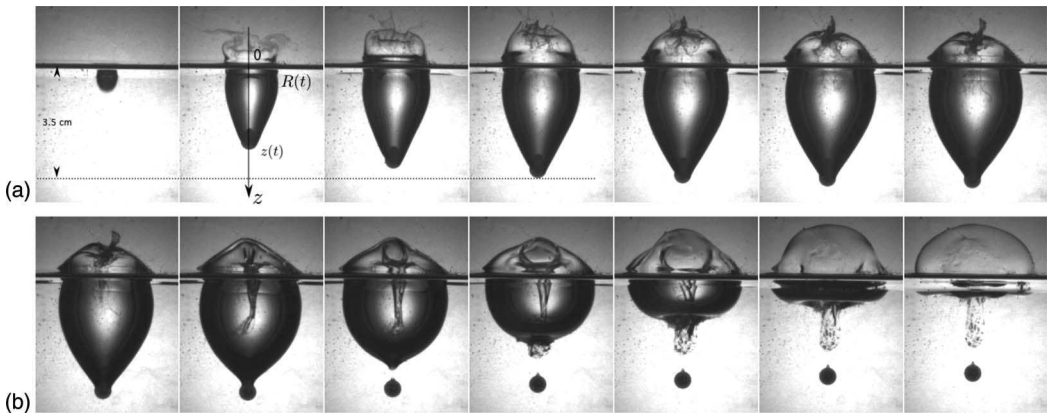

FIG. 2. Chronophotography of the impact of a polypropylene sphere (radius $R_0 = 3.5$ mm) onto a bath of silicon oil ($\eta = 1000$ mPa s) at $V_0 = 28$ m/s. The first row of pictures shows the rapid opening of the cavity (interval Δt between two snapshots is 2.8 ms), while the second row represents its slower decay ($\Delta t = 16$ ms) (movie is slowed down 250 times) (enhanced online). [URL: http://dx.doi.org/10.1063/1.4797499.1]

III. DRAG FORCE

In Figure 3, we present the evolution of the velocity of a polypropylene sphere ($R_0 = 2.5$ mm) hitting the oil at $V_0 = 20$ m/s. As in Figure 2, we observe that the velocity strongly decreases within 5 ms: the associated Reynolds number $Re = \frac{\rho R_0 V}{\eta}$ falls from $Re_0 = 100$ to $Re = 1$ in this period of time. To get a deceleration law, we need an expression for the drag force. We assume that the drag is the same as for spheres without cavity at similar Reynolds numbers. To justify this assumption, we note that May and Woodhull[21] studied the variation of drag force in water entry as a function of Reynolds number in the range $Re \sim 10^4$–10^6. Despite the presence of a cavity behind the sphere, the relationship between the drag coefficient and the Reynolds number, $C_D(Re)$, was found very similar to the one obtained in a continuous Newtonian fluid.[22] We extend this result to Reynolds numbers smaller than 100. In this range, the drag force is determined by a "skin" friction, that is, the friction associated to the boundary layer δ : $F \sim \eta \frac{V}{\delta} R_0^2$, with $\delta \sim \sqrt{\eta R_0/\rho V}$ the typical boundary layer thickness.[23] The Stokes regime ($F \sim \eta V R_0$) is reached when δ becomes comparable to the sphere radius R_0, i.e., when the Reynolds number gets smaller than unity. For $R_0 = 2.5$ mm and $\eta = 1$ Pa s, one enters this viscous regime at a velocity $V = \eta/\rho R_0 \approx 0.4$ m/s. The initial deceleration phase in Figures 2 and 3(a) is thus out of the Stokes regime.

With the expression for the skin friction, the equation of motion can be written

$$\frac{4}{3}\pi R_0^3 \rho_s \frac{dV}{dt} = -\alpha\sqrt{\rho\eta R_0^3 V^3}. \tag{1}$$

The coefficient α was measured in wind tunnels[22] and found to be close to 13. In our case, since the cavity prevents friction over half of the surface, we expect $\alpha \approx 6.5$. In addition, we have neglected buoyancy in (1). This assumption is valid as long as the friction $\sqrt{\rho\eta R_0^3 V^3}$ exceeds the Archimedean force $(\rho_s - \rho) R_0^3 g$. This condition implies that Eq. (1) only holds above a velocity $V_b = \left[(\rho_s/\rho - 1)^2 \rho R_0^3 g^2/\eta\right]^{1/3}$. For all our experiments, V_b is smaller than 1m/s, so that Eq. (1) is expected for the initial deceleration phase. Using the relation $V = dz/dt$ between the velocity and the vertical location of the sphere defined in Figure 2, we can integrate Eq. (1) and predict the evolution of the velocity with the depth. We find

$$\sqrt{\frac{V}{V_0}} = 1 - \frac{z}{z^*}. \tag{2}$$

In this equation, $z^* = \frac{8\pi}{3\alpha}\mathcal{L} \approx 1.3\mathcal{L}$ is the distance at which the sphere stops, with

$$\mathcal{L} = R_0 \frac{\rho_s}{\rho}\sqrt{Re_0}. \tag{3}$$

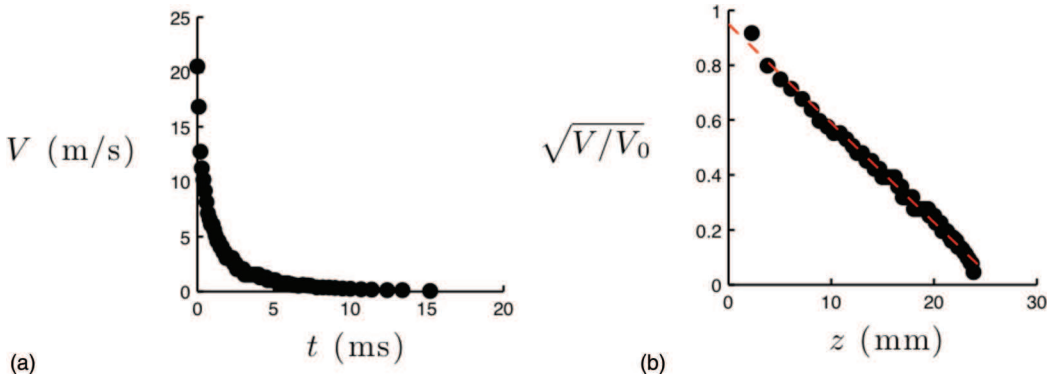

FIG. 3. Deceleration of a polypropylene sphere ($R_0 = 2.5$ mm) arriving at $V_0 = 20$ m/s onto a bath of silicon oil ($\eta = 1$ Pa s): the velocity is plotted as a function of time t in (a) and the quantity $\sqrt{V/V_0}$ as a function of distance z in (b). The dashed line represents the best linear fit (Eq. (2)), with $z^* \approx 26$ mm.

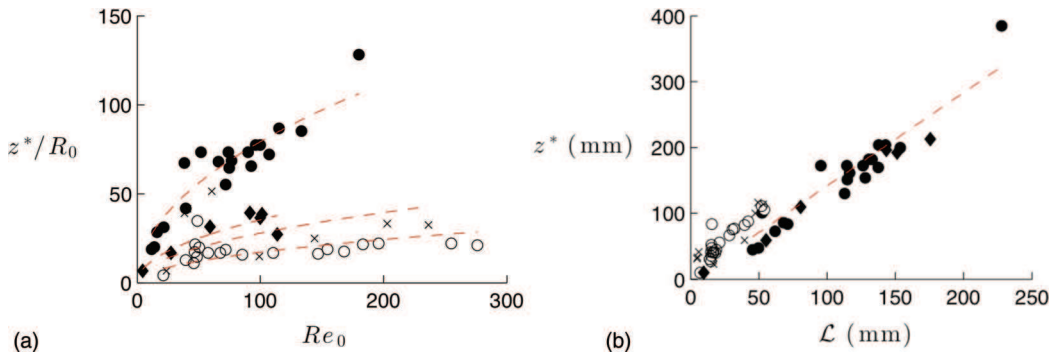

FIG. 4. Arrest distance $z^\star$ deduced from experiments, as a function of the impact parameters. (a) z^*/R_0 is plotted as a function of the Reynolds number at impact $Re_0 = \rho V_0 R_0/\eta$ and (b) experimental arrest length z^* presented as a function of the characteristic length $\mathcal{L} = R_0 \frac{\rho_s}{\rho}\sqrt{Re_0}$. The different symbols correspond to different materials: polypropylene (○), polyacetal (×), stainless steel (●), and glass (⧫) spheres.

For the parameters corresponding to Figure 1 ($R_0 = 2.5$ mm, $\rho_s \simeq \rho$, and $Re_0 = 70$), the characteristic distance z^* is on the order of 3 cm, indeed comparable to our observations. We eventually plot in Figure 3(b) $\sqrt{V/V_0}$ as a function of z for the data of Figure 3(a). A linear decrease is observed, as expected from Eq. (2), from which we deduce an arrest distance $z^* \approx 26$ mm.

This procedure to measure z^* was repeated and we show in Figure 4(a) the reduced arrest length z^*/R_0 as a function of the Reynolds number at impact, for different sphere densities. For each density, a parabolic behavior (shown by a dashed line) is found to fit the data, as expected from Eq. (3). The same data set is used in Figure 4(b) where the arrest length z^* is plotted as a function of the characteristic length $\mathcal{L}$ given by Eq. (3). This representation makes all the data collapse on a single line of slope 1.3.

IV. SHAPE OF THE CAVITY

As can be seen in Figure 3, the distance z^* fixes the depth of the cavity, in sharp contrast with fast impacts in water, for which oblong cavities pinch before projectiles stop.[10,20,24] Here, z^* scales as $R_0\sqrt{Re_0}\rho_s/\rho$, independent of g and only fixed by the sphere radius, the density ratio, and initial Reynolds number. Logically, this behavior differs from the scaling in usual water-entry problems, for which the length of the cavity H is found to scale as $R_0 V_0/\sqrt{gR_0}$, thus independent of the density ratio and viscosity, and function of the Froude number ($Fr = \frac{V_0^2}{gR_0}$), as confirmed with spheres[10] and disks.[6,7]

We do not model our cavities in their whole complexity but simplify them as cylinders of radius R and height z and discuss the evolution of the aspect ratio z/R. Since gravity does not influence significantly their formation, we assume that energy is dissipated isotropically. This assumption is compatible with the flow characteristics shown in Figure 5. Isotropy of the flow implies that the energy $F.V$ dissipated per unit of time in the longitudinal direction is of the order of the energy $\eta\left(\dot{R}/R\right)^2 R^2 z$ dissipated per unit of time in the transverse direction. Using the expression of the friction force F discussed in Sec. III, this isotropic argument leads to the equation

$$\dot{R}^2 z \simeq \sqrt{\frac{\rho R_0^3 V^5}{\eta}}. \tag{4}$$

Substituting V by its expression in Eq. (2), and using the fact that $\dot{R} \simeq \frac{dR}{dz}V$, we get an equation for $R(z)$:

$$\frac{dR}{dz} = \left(\frac{\rho V_0 R_0^3}{\eta z^{*2}}\right)^{1/4}\sqrt{\frac{1-z/z^*}{z/z^*}} = \sqrt{\frac{\rho}{\rho_s}\,\frac{1-z/z^*}{z/z^*}}. \tag{5}$$

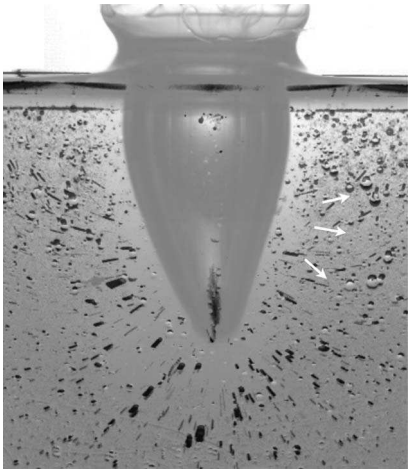

FIG. 5. Visualisation of the flow around the cavity created by a polypropylene sphere with $R_0 = 2.5$ mm and $V_0 = 24$ m/s. The motion in the oil is visualized using small trapped air bubbles and superimposing 1.6 ms of experiment. The white arrows underline the direction of the velocity vector. The image is taken 3 ms after impact.

To simplify the notations, we define the dimensionless depth $Z = z/z^*$ and integrate (5), which yields an expression for the aspect ratio of the cavity:

$$\frac{z}{R} \simeq \sqrt{\frac{\rho_s}{\rho}} \frac{Z}{\arcsin\sqrt{Z} + \sqrt{Z(1-Z)}}. \tag{6}$$

According to Eq. (6), the aspect ratio is a universal function of the relative location $Z = z/z^*$, apart from its sensitivity to the density ratio ρ_s/ρ.

Experimentally, we define the aspect ratio of a viscous cavity as that of the cylinder in which it can be enclosed, which can be measured on each picture of a sequence. The vertical extension is always the current depth z, while the radial extension R corresponds to the radius of the widest region of the vase. In Figure 6, we show the evolution of two cavities obtained with two different velocities, namely 12.8 m/s (top sequence) and 25.9 m/s (bottom sequence). Despite a factor 4 in the initial kinetic energy, the aspect ratios are similar.

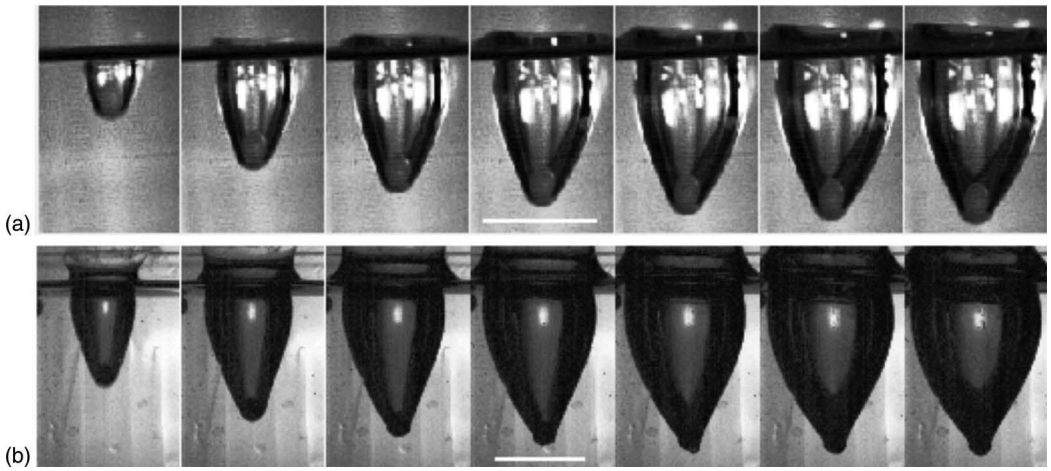

FIG. 6. Chronophotographies of the cavity after the impact of a polypropylene sphere ($R_0 = 2.5$ mm, $\rho_s = 920$ kg/m^3) at different velocities: (a) $V_0 = 12.8$ m/s with $\Delta t = 1.4$ ms and (b) $V_0 = 25.9$ m/s with $\Delta t = 1.25$ ms. The bars indicate 2 cm.

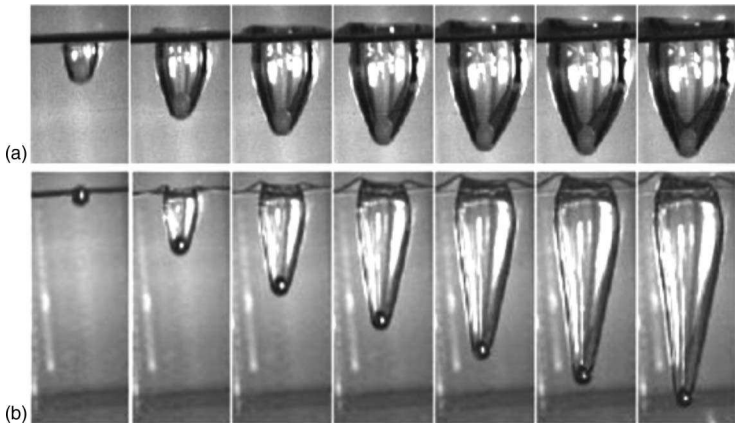

FIG. 7. Chronophotography of the impact of two spheres with $R_0 = 2.5$ mm, $V_0 = 13$ m/s, and different densities: (a) polypropylene, $\rho_s = 920$ kg/m^3 and (b) stainless steel, $\rho_s = 7700$ kg/m^3.

Equation (6) also suggests that the aspect ratio increases with the sphere density. This effect is illustrated in Figure 7 where two spheres of identical radius and impact velocity hit a bath of silicon oil V1000. We observe that steel (sequence (b)) produces a more elongated cavity than polypropylene (sequence (a)). The ratio of density is increased by a factor 8 and the difference of aspect ratio is compatible with a square root dependency ($\sqrt{8} \approx 2.8$). More quantitatively, we present in Figure 8(a) the evolution of the aspect ratio z/R as a function of the relative location z/z^* for different densities. Again, the steel sphere produces a cavity more elongated than the plastic one. Moreover, at small z, the data follow a parabolic law (dashed lines), as expected from an expansion of (6) at small Z, which gives $z/R \sim \sqrt{\frac{\rho}{\rho_s}}\, Z$.

According to (6), the rescaled aspect ratio $\frac{z}{R}\sqrt{\frac{\rho}{\rho_s}}$ should only be a function of relative location $Z = z/z^*$. Using the data set presented in Figure 8(a), we show in Figure 8(b) that the data do collapse on a single curve, close to the theoretical dashed line given by Eq. (6). The agreement is satisfactory up to $z/z^* \leq 0.6$. Above this limit, according to Eq. (2), the velocity of the sphere has been reduced by 90% ($V/V_0 = 0.1$) and the effects that we have neglected such as buoyancy become important.

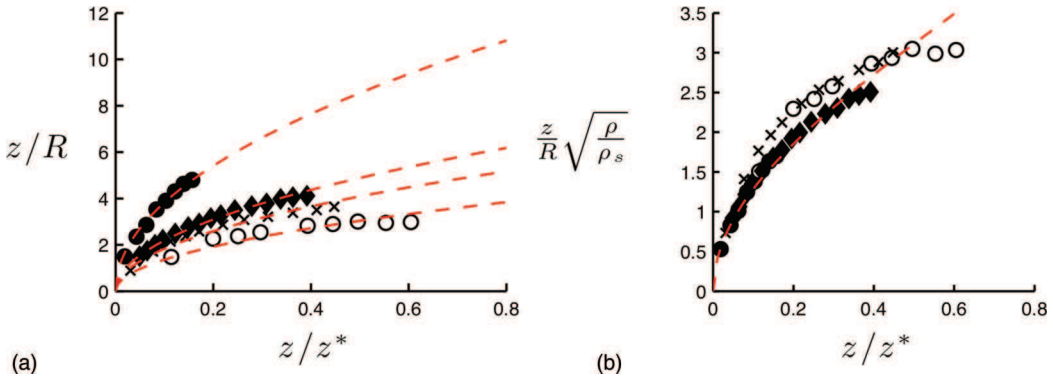

FIG. 8. (a) Instantaneous aspect ratio z/R of the cavity, plotted as a function of its normalized depth $Z = z/z^*$. Dashed lines are square root fits, as expected from Eq. (6) at low Z. Spheres are made of polypropylene (○), polyacetal (×), stainless steel (●), and glass (♦). (b) Data collapse on the same curve when z/R is corrected by a factor $\sqrt{\frac{\rho}{\rho_s}}$. The dashed line represents the function $Y = a\frac{Z}{\arcsin\sqrt{Z}+\sqrt{Z(1-Z)}}$, with $a = 5.75$.

V. CONCLUSION

We reported here various characteristics of solid impacts in viscous liquids. We showed that large velocity impacts dig transient holes that are different from cavities in water: the shape does not depend on gravity, but is all determined by the density ratio and Reynolds number. A model based on skin friction allowed us to predict the depth of the cavity, while assuming an isotropic energy dissipation made it possible to recover most of the geometrical salient features of these viscous holes.

[1] A. M. Worthington and R. S. Cole "Impact with a liquid surface studied by the aid of instantaneous photography. Paper II," Philos. Trans. R. Soc. London, Ser. A **194**, 175–199 (1900).
[2] E. G. Richardson, "The impact of a solid on a liquid surface," Proc. Phys. Soc. **61**, 352–367 (1948).
[3] G. Birkhoff and E. H. Zarantonello, *Jets, Wakes and Cavities* (Academic Press Inc., New York, 1957).
[4] J. M. Oliver, "Water entry and related problems," Ph.D./DPhil dissertation (University of Oxford, 2002).
[5] T. von Karman, "The impact on seaplane floats during landing" in NACA-TN-316, National Advisory Committee for Aeronautics, Washington, DC, 1929.
[6] J. W. Glasheen and T. A. McMahon, "Vertical water entry of disks at low Froude numbers," Phys. Fluids **8**, 2078–2083 (1996).
[7] J. W. Glasheen and T. A. McMahon, "A hydrodynamic model of locomotion in the basilisk lizard," Nature (London) **380**, 340–342 (1996).
[8] C. Duez, C. Ybert, C. Clanet, and L. Bocquet, "Making a splash with water repellency," Nat. Physics **3**, 180–183 (2007).
[9] T. T. Truscott, and A. H. Techet, "Water entry of spinning spheres," J. Fluid Mech. **625**, 135–165 (2009).
[10] V. Duclaux, F. Caillé, C. Duez, C. Ybert, L. Bocquet, and C. Clanet, "Dynamics of transient cavities," J. Fluid Mech. **591**, 1–19 (2007).
[11] R. Bergmann, D. van der Meer, S. Gekle, A. van der Bos, and D. Lohse, "Controlled impact of a disk on a water surface: Cavity dynamics," J. Fluid Mech. **633**, 381–409 (2009).
[12] S. T. Thoroddsen and A. Q. Shen, "Granular jets," Phys. Fluids **13**, 4–6 (2001).
[13] J. S. Uehara, M. A. Ambroso, R. P. Ojha, and D. J. Durian, "Low-speed impact craters in loose granular media," Phys. Rev. Lett. **90**, 194301 (2003).
[14] D. Lohse, R. Bergmann, R. Mikkelsen, C. Zeilstra, D. van der Meer, M. Versluis, K. van der Weele, M. van der Hoef, and H. Kuipers, "Impact on soft sand: void collapse and jet formation," Phys. Rev. Lett. **93**, 198003 (2004).
[15] J. R. Royer, E. I. Corwin, A. Flior, M. L. Cordero, M. L. Rivers, P. J. Eng, and H. M. Jaeger, "Formation of granular jets observed by high-speed X-ray radiography," Nat. Phys. **1**, 164–167 (2005).
[16] A. Le Goff, "Impact figures," Ph.D. dissertation (Université Pierre et Marie Curie, Paris, 2009).
[17] T. Podgorski and A. Belmonte, "Surface folds during the penetration of a viscoelastic fluid by a sphere," J. Fluid Mech. **460**, 337–348 (2002).
[18] B. Akers and A. Belmonte, "Impact dynamics of a solid sphere falling into a viscoelastic micellar fluid," J. Non-Newtonian Fluid Mech. **135**, 97–108 (2006).
[19] P. Dontula, C. W. Macosko, and L. E. Scriven, "Does the viscosity of glycerin fall at high shear rates?," Ind. Eng. Chem. Res. **38**, 1729–1735 (1999).
[20] J. M. Aristoff and J. W. M. Bush, "Water entry of small hydrophobic spheres," J. Fluid Mech. **619**, 45–78 (2009).
[21] A. May and J. C. Woodhull, "Drag coefficient of steel spheres entering water vertically," J. Appl. Phys. **19**, 1109–1121 (1948).
[22] H. Schlichting and K. Gersten, *Boundary Layer Theory* (Springer-Verlag, Berlin, 2000).
[23] L. Prandtl, "Motion of fluids with very little viscosity," in Technical Memorandum 452, National Advisory Committee for Aeronautics, Washington, DC, 1928.
[24] M. Lee, R. G. Longoria, and D. E. Wilson, "Cavity dynamics in high-speed water entry," Phys. Fluids **9**, 540–550 (1997).